Effect of Uniaxial Compression on Impurity Conduction in p-Germanium*†

FRED H. POLLAK‡§
Department of Physics and Institute for the Study of Metals, University of Chicago, Chicago, Illinois
(Received 20 November 1964)

The effect of uniaxial compression along [100] and [111] on impurity conduction has been investigated in Ga-doped p-Ge in the concentration range $3\times10^{15}<N_A<9\times10^{16}$ cm^{-3} for compensation $K=0.04$ and in the range $9\times10^{14}<N_A<4\times10^{16}$ cm^{-3} for $K=0.40$. The experiments were performed between 300 and 1.2°K. The largest stress applied was 6.8×10^9 dyn cm^{-2}. The analysis of the experimental results deals primarily with the high-stress region ($X>4\times10^9$ dyn cm^{-2}) in which the two valence bands, which in the absence of stress are degenerate at $\mathbf{k}=0$, are nearly decoupled so that the effect of the lower band on the acceptor wave function is treated as a perturbation. In the low-concentration region ($N_A<5\times10^{15}$ cm^{-3}) the extension of Miller and Abrahams' theory to include nonspherical charge distributions, together with the acceptor wave functions calculated from the effective-mass approximation, accounts for the observed stress dependence of the resistivity. At intermediate concentrations ($2\times10^{16}<N_A<9\times10^{16}$ cm^{-3}) a linear relation between the impurity-conduction activation energy ϵ_2 and the acceptor ionization energy ϵ_1 is established. Although the experimental results are not able to distinguish between Mikoshiba's and Frood's theories of the ϵ_2 process they are clearly in disagreement with the predictions of Mycielski's theory. The investigation of the stress dependence of the transition from nonmetallic to metallic conduction yields the stress dependence of the effective Bohr radius. The form of this stress dependence indicates the importance, at high concentrations, of the potential-energy term in the effective-mass Hamiltonian. This term can be neglected at low concentrations.

I. INTRODUCTION

IT has been shown in n-Ge that the size and shape of the donor wave functions are greatly changed by the application of a uniaxial stress,[1–3] which removes the degeneracy of the four [111] conduction-band valleys. This stress-induced change of the donor wave function was observed to have a considerable effect on impurity conduction, which depends sensitively on the overlap of the wave functions of neighboring impurities. From these studies information was obtained about the detailed structure of the donor states and about the effect of the valley-orbit splitting energies.

The purpose of this work is to report similar studies on p-Ge in which the stress-induced change of the acceptor wave function results from the splitting of the heavy and light hole valence bands which at zero stress are degenerate at $\mathbf{k}=0$.

Because of the different types of degeneracies occurring at the extrema of the conduction and valence bands quite a different behavior of impurity conduction as a function of stress is expected in p-Ge as compared to n-Ge.

The investigation of the stress dependence of impurity conduction in p-Ge is expected to yield information in two different ways. First, by relying on the aspects of impurity conduction which are understood one can test the approximations needed to obtain the stress-dependent acceptor wave functions from the change of the valence band structure. Secondly, by reversing the arguments and relying on our knowledge of the acceptor wave function one can obtain information about the process of impurity conduction in the range of intermediate and higher impurity concentrations for which no satisfying theory exists at present.

Since impurity conduction and its stress dependence exhibit quite different properties in the different concentration ranges,[4] we shall briefly describe the properties of impurity conduction and define four concentration regions as they are used in this paper. A more detailed account of the experimental and theoretical status of impurity conduction can be found in the review article by Mott and Twose.[5]

It has been shown that in the temperature range $77°\text{K}<T<1°\text{K}$ the temperature dependence of the resistivity ρ can be approximated by the sum of three exponential terms[6]

$$\rho^{-1}=\sum_{i=1}^{3}\rho_i^{-1}\exp(-\epsilon_i/kT), \qquad (1)$$

where ϵ_1 is the acceptor ionization energy. In Fig. 1 the impurity-conduction activation energies ϵ_2 and ϵ_3, at zero stress, for low-compensation[4] Sb and Ga-doped Ge are plotted as a function of average impurity separation R. Figure 4 of Ref. 7 shows ϵ_3 as a function of R for compensation $K=0.40$. (At these high compensations ϵ_2 does not appear.)

In *low-concentration region I* (LCR I; $N_A<5\times10^{15}$ cm^{-3}) impurity conduction exhibits only activation

* Submitted as a thesis in partial fulfillment of the requirements for the degree of Doctor of Philosophy at the University of Chicago.

† Supported in part by the U. S. Air Force Office of Scientific Research through grant number AFOSR 62-178.

‡ Gulf Oil Predoctoral Fellow (1961–62) and National Lead Predoctoral Fellow (1962–63).

§ Present address: Physics Department, Brown University, Providence, Rhode Island.

[1] H. Fritzsche, Phys. Rev. **119**, 1899 (1960).
[2] H. Fritzsche, Phys. Rev. **125**, 1552 (1962).
[3] H. Fritzsche, Phys. Rev. **125**, 1560 (1962).
[4] H. Fritzsche, J. Phys. Chem. Solids **6**, 69 (1958).
[5] N. F. Mott and W. D. Twose, Suppl. Phil. Mag. **10**, 107 (1961).
[6] H. Fritzsche, Phys. Rev. **99**, 406 (1955).
[7] H. Fritzsche and M. Cuevas, Phys. Rev. **119**, 1238 (1960).

energy ϵ_3, which is inversely proportional to R (see Fig. 1). Several theoretical studies,[8–10] particularly that of Miller and Abrahams (MA), have been quite successful in this region. These theories are based on the model of phonon-induced charge tunneling between impurity sites, where a fraction K of the sites is vacant because of compensation. Since ρ_3 is inversely proportional to the tunneling probability an investigation of its stress dependence yields information concerning the stress dependence of the effective Bohr radius. (The use of the term "effective Bohr radius" is discussed in Sec. IV-A-4.) The stress dependence of ϵ_3 has been investigated to determine whether this activation energy is independent of wave-function size and caused only by the Coulomb interaction of the carriers with the compensating impurity ions.[11]

Also in *low-concentration region II* (LCR II; $5\times10^{15}<N_A<2\times10^{16}$ cm^{-3}) impurity conduction exhibits only ϵ_3 but in this region it deviates from the Coulombic $1/R$ dependence. This suggests that, because of the greater overlap of impurity wave functions in this region, the resonance energy between sites is no longer much smaller than the variation in local electric fields, as was assumed in the theories of LCR I. The stress dependence of ϵ_3 has been measured and is compared to its stress dependence in LCR I and at intermediate concentrations. The stress dependence of ρ_3 is compared to the theory of MA to determine whether the theory is still valid for ρ_3 in this region.

In the *intermediate-concentration region* (ICR; $2\times10^{16}<N_A<9\times10^{16}$ cm^{-3}) impurity conduction exhibits both activation energies ϵ_2 and ϵ_3. In this concentration region the conduction process is least understood. Several theories[12–14] have predicted a linear relationship between ϵ_2 and ϵ_1. It has been found experimentally that (1) ϵ_2 is a sensitive function of R (see Fig. 1) and of the effective Bohr radius[2] and (2) in contrast to the low-concentration regions ϵ_3 in this region, like ϵ_2, decreases as R decreases. Therefore, the ability to change ϵ_1[15,16] and the effective Bohr radius by means of a uniaxial stress may help explain these conduction processes.

At *high concentrations* ($N_A>1\times10^{17}$ cm^{-3}) a transition from nonmetallic to metallic conduction is defined to occur when $\epsilon_2=0$. The value of R/a, where a is the effective Bohr radius, at which this transition occurs is predicted to be constant.[5] Therefore, information concerning the stress dependence of a is obtained by investigating the stress dependence of this transition.

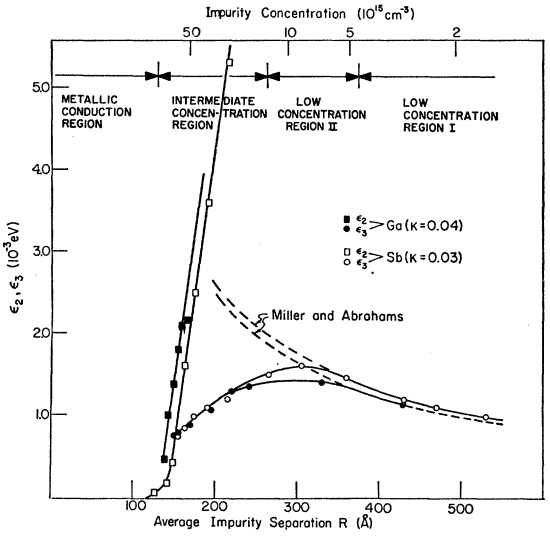

FIG. 1. Activation energies ϵ_2 and ϵ_3 for low-compensation Sb and Ga-doped Ge as a function of average impurity separation and impurity concentration. The dashed lines represent ϵ_3 as calculated from Miller and Abrahams' theory. $K=N_D/N_A$ is the compensation ratio.

In unstressed p-Ge the effective-mass theory of the acceptor wave function is complicated because of the degeneracy of the two valence bands at $\mathbf{k}=0$.[17–19] The application of a uniaxial stress removes this degeneracy and separates the two bands by an energy proportional to the stress.[15,16,20,21] In the high-stress region the two bands are nearly decoupled so that the effect of the lower band on the acceptor wave function can be treated as a perturbation. Therefore, first-order correction terms to quantities which are dependent on the impurity wave function will be proportional to $1/X$. For large compressional stress along [100] or [111] the envelope function of the acceptor ground-state wave function is cigar shaped with the axis of rotation along the direction of stress[15,16] so that stress along these two directions will produce qualitatively similar results. Because of the relative simplicity of the wave function at high stresses the interpretation of the experimental results in this region is considerably easier than at low stresses.

Sugiyama and Kobayashi[22] have investigated the effect of compression along [100] on impurity conduction for Ga-doped Ge. However, the largest stress applied was only 2×10^9 dyn cm^{-2} and measurements on only one sample, which is in the metallic region at zero stress, are reported. The object of this work is to study the effect of uniaxial compression along [100] and [111]

[8] A. Miller and E. Abrahams, Phys. Rev. **120**, 745 (1960).
[9] T. Kasuya and S. Koide, J. Phys. Soc. Japan **13**, 1287 (1958).
[10] W. D. Twose, thesis, Cambridge, 1959 (unpublished).
[11] N. F. Mott, Can. J. Phys. **34**, 1356 (1956).
[12] N. Mikoshiba (private communication). This theory is based on a suggestion made in Ref. 4.
[13] D. G. H. Frood, Proc. Phys. Soc. (London) **75**, 185 (1960).
[14] J. Mycielski, Phys. Rev. **123**, 99 (1961).
[15] P. J. Price, Phys. Rev. **124**, 713 (1961).
[16] J. J. Hall, Phys. Rev. **128**, 68 (1962).
[17] J. M. Luttinger and W. Kohn, Phys. Rev. **97**, 869 (1955).
[18] W. Kohn and D. Schechter, Phys. Rev. **99**, 1903 (1955).
[19] D. Schechter, J. Phys. Chem. Solids **23**, 237 (1962).
[20] G. E. Picus and G. L. Bir, Fiz. Tverd. Tela **1**, 154 (1959); **1**, 1642 (1959) [English transl.: Soviet Phys.—Solid State **1**, 136 (1959); **1**, 1502 (1960)].
[21] H. Hasegawa, Phys. Rev. **129**, 1029 (1963).
[22] K. Sugiyama and A. Kobayashi, J. Phys. Soc. Japan **18**, 163 (1963).

on impurity conduction, particularly in the high-stress region ($X>4\times10^9$ dyn cm^{-2}) in which the two valence bands are almost decoupled. Specifically, we have investigated the stress dependence of (1) ρ_3 and ϵ_3 in LCR I and II, (2) ϵ_2 and ϵ_3 in ICR, and (3) the transition from nonmetallic to metallic conduction. The experiments were performed at temperatures between 300 and 1.2°K. The largest stress applied was 6.8×10^9 dyn cm^{-2}. The resistivity was measured for current flow parallel to the stress direction, except for one sample (Ga-16) for which the current and stress directions were perpendicular.

II. EXPERIMENTAL DETAILS

All samples were cut from single crystals perpendicular to the growth axis to minimize the impurity concentration gradient along their length. Wafers about 1 mm thick were first cut from the crystal and then strips about 1 mm wide were cut from the wafer along the direction to be stressed. Samples Ga-15 and Ga-16 are adjacent strips from the same wafer. The orientation was by x rays to better than one degree.

The surface treatment, mounting of samples, cryostat, and stressing arrangement have been described before.[23] However, two modifications have been made. (1) The samples were cemented into brass cups with epoxy cement. (2) Instead of weights a spring was used to apply the stress. A Schaevitz linear variable differential transformer (LVDT) was mounted inside the spring and a matched LVDT was mounted on a micrometer, having 0.0001-in. graduations, outside the system. The two LVDT's were connected as the two arms of an ac bridge, the null being detected by a vacuum-tube voltmeter. The output voltage per displacement of the LVDT's was matched to 0.15%.

TABLE I. Sample characteristics.

Sample	K	ρ(300°K) (Ω-cm)	ρ(78°K) (Ω-cm)	ρ(4.2°K) (Ω-cm)	N_A (cm^{-3})	R (Å)
Ga-1	0.04	5.03	0.466	9.63×10^7	9.5×10^{14}	630±10
Ga-2	0.04	1.23	0.148	9.01×10^5	3.0×10^{15}	430±7
Ga-3	0.40	1.19	0.196	1.69×10^4	6.8×10^{15}	330±6
Ga-4	0.04	0.576	0.111	1.65×10^4	6.6×10^{15}	330±6
Ga-5	0.04	0.557	0.111	1.35×10^4	7.0×10^{15}	320±6
Ga-6	0.40	0.194	0.0844	18.9	4.2×10^{16}	180±3
Ga-7	0.04	0.253	0.0644	1.24×10^4	1.7×10^{16}	240±4
Ga-8	0.04	0.216	0.0605	8.51×10^3	2.2×10^{16}	220±4
Ga-9	0.04	0.215	0.0604	8.26×10^3	2.2×10^{16}	220±4
Ga-10	0.04	0.146	0.0519	1.26×10^3	3.2×10^{16}	195±3
Ga-11	0.04	0.141	0.0519	1.05×10^3	3.2×10^{16}	195±3
Ga-12	0.04	0.108	0.0459	1.91×10^2	4.8×10^{16}	170±3
Ga-13	0.04	0.0957	0.0436	74.8	5.3×10^{16}	165±3
Ga-14	0.04	0.0898	0.0432	60.4	6.0×10^{16}	160±3
Ga-15	0.04	0.0875	0.0431	21.2	6.2×10^{16}	155±3
Ga-16	0.04	0.0870	0.0431	25.0	6.2×10^{16}	150±3
Ga-17	0.04	0.0787	0.0402	11.2	7.0×10^{16}	150±3
Ga-18	0.04	0.0677	0.0395	3.78	8.2×10^{16}	142±2
Ga-19	0.04	0.0633	0.0384	0.971	9.0×10^{16}	138±2

[23] H. Fritzsche, Phys. Rev. 115, 336 (1959).

The reproducibility of the piezoresistance effect was repeatedly checked and found to be better than 1%.

III. EXPERIMENTAL RESULTS

Table I lists the samples used in this experiment with their compensation ratio K, resistivity ρ at 300, 78, and 4.2°K, acceptor concentration N_A, and average acceptor separation R. The properties of the samples with $K=0.40$ have already been described.[7] K for Ga-2 was determined by fitting ϵ_3 at zero stress to

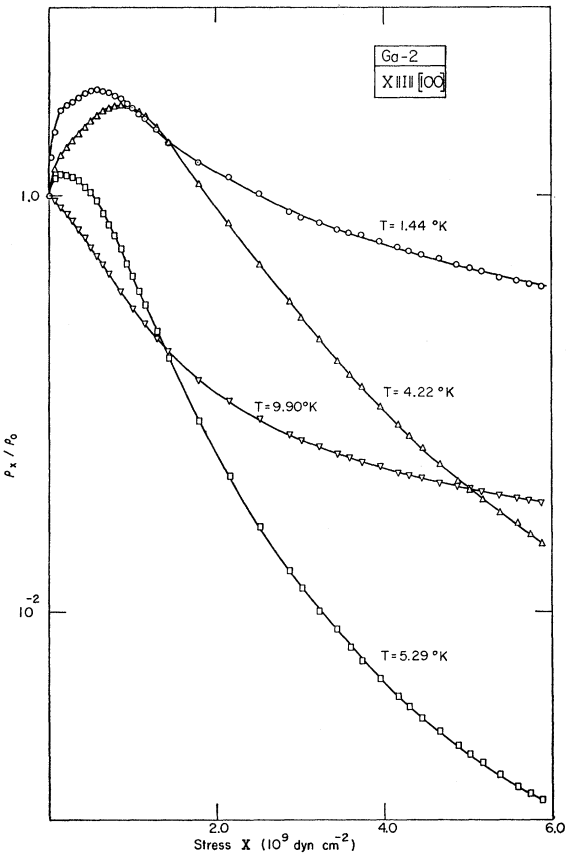

FIG. 2. Ratio of the resistivity with stress to the value without stress of Ga-2 as a function of uniaxial compressional stress along [100]. The three lowest temperatures are in the impurity-conduction region while 9.90°K is the ϵ_1 region.

Eq. (25). The other samples of low compensation are assumed to have the same K. N_A was determined from the resistivity at 300°K.[24] The error in this determination is about 5%. R was calculated using the relation $R=(3/4\pi N_A)^{1/3}$.

A. Stress Parallel to [100]

1. Low-Concentration Region I

Figure 2 shows ρ_X/ρ_0 as a function of compressional stress X for Ga-2 at various temperatures, where ρ_X

[24] W. W. Tyler and T. J. Soltys (private communication).

and ρ_0 are the resistivities with and without stress, respectively. For the same sample Fig. 3 shows the resistivity ρ as a function of $1/T$ for various stresses. This curve exhibits acceptor ionization energy ϵ_1 and impurity conduction activation energy ϵ_3. The stress dependence of ϵ_1 has been measured and in the high-stress region is given by[15,16]

$$\epsilon_1(X)=\epsilon_1(\infty)+A_1/X. \quad (2)$$

The values of $\epsilon_1(\infty)$ and A_1 for compressional stress along [100] and [111] for Al and In impurities are listed in Table II.

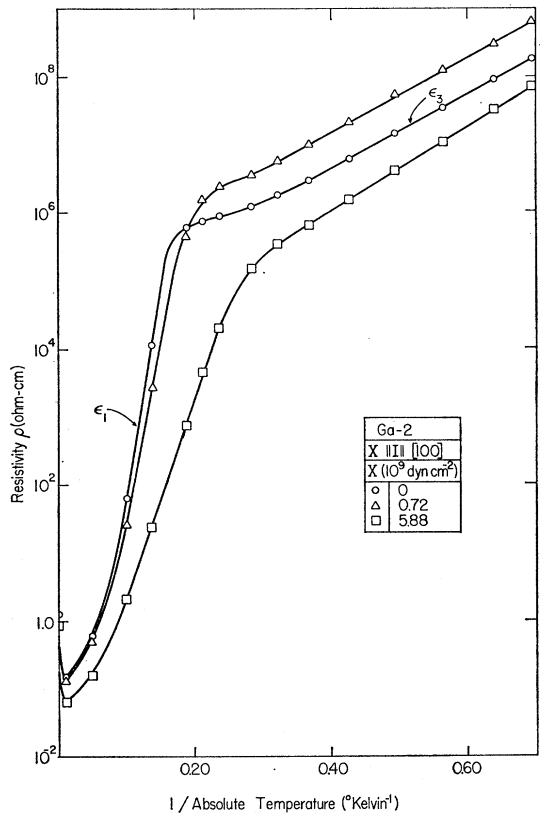

FIG. 3. Resistivity of Ga-2 for various [100] compressional stresses as a function of $1/T$. The range of impurity conduction extends from about 5°K to the lowest temperatures.

In the low-temperature region, where impurity conduction is observed, ρ_X/ρ_0 increases, reaches a maximum and then decreases as the stress is increased. At higher temperatures, where ϵ_1 is observed, the resistivity decreases monotonically. This behavior is typical of all samples measured. Because of the complexity of the acceptor wave function at low stresses little can be said about its stress dependence although the increase in resistivity suggests that the wave function is contracting with increasing stress in this stress region. As will be shown in the next section, in the high-stress region the envelope function of the upper band is

TABLE II. Experimental values of $\epsilon_1(\infty)$ and A_1.

Sample	Stress direction	$\epsilon_1(\infty)$[a] (10^{-3} eV)	A_1[a] (10^6 eV dyn cm^{-2})
Al-30	[100]	4.75±0.15	11.7±1.6
In-71	[100]	4.78±0.15	13.5±1.6
Al-30	[111]	6.30±0.15	8.4±2.1
In-71	[111]	6.76±0.15	9.8±1.7

[a] Reference 16.

expanding with increasing stress causing the resistivity in the impurity conduction region to decrease. Since ϵ_1 decreases monotonically as a function of stress[15,16] so does the resistivity in this temperature range. Table III lists $(\rho_X/\rho_0)_{max}$ and the stress for which it occurs for two temperatures, 4.2°K and the lowest temperature measured for that particular sample. In this concentration region $(\rho_X/\rho_0)_{max}$ is not very temperature-dependent and the stress for which it occurs shifts to slightly lower values as the temperature decreases

As shown in Fig. 3, in the impurity conduction region, the effect of the stress is to change both ϵ_3 and $\ln\rho_3$,[25] the intercept of the extrapolated $\ln\rho$ versus $1/T$ curve to $1/T=0$. These quantities were determined by a least-squares fit of $\ln\rho$ versus $1/T$ for $T<2.5$°K. The deviation from linearity was less than 0.25%. The plateau which appears in the curve at about 5°K, the high-temperature end of the impurity-conduction region, gradually disappears as the stress increases. This plateau, which has been explained as a saturation in the carrier concentration,[17] has been observed for both acceptors[6,7] and donors[4] but is more prominent in samples of low compensation and concentration. Because of the decrease of ϵ_1 with stress, the onset of impurity conduction moves to temperatures which are lower than the saturation temperature and hence the plateau disappears.

In Fig. 4 $\ln\rho_3$ and ϵ_3 are plotted as a function of $1/X$ in the high-stress region ($X>4\times10^9$ dyn cm^{-2}). With increasing stress $\ln\rho_3$ decreases while ϵ_3 increases. The decrease in $\ln\rho_3$ is caused by the expanding wave function. The fact that ϵ_3 is stress-dependent means that it is no longer due to a simple Coulomb interaction.[11] Since both quantities are linear in $1/X$ one can write

$$\epsilon_3(X)=\epsilon_3(\infty)+A_3/X, \quad (3)$$

$$\ln\rho_3(X)=\ln\rho_3(\infty)+B_3/X. \quad (4)$$

This linear relationship was found also for Ga-1.

Table IV lists the experimental values of $\epsilon_3(\infty)$, A_3, $\ln\rho_3(\infty)$, and B_3. It should be noted that A_3 is negative.

2. *Low-Concentration Region II*

In this concentration region the behavior of the resistivity as a function of stress is similar to LCR I. In

[25] The quantity ρ_3 has the dimensions of resistivity and will always be given in units of Ω cm.

TABLE III. $(\rho_X/\rho_0)_{max}$ and the stress X for which it occurs at 4.2°K and at the lowest temperature. The concentration region in which the sample belongs is listed in parenthesis.

Sample	K	R (Å)	$(\rho_X/\rho_0)_{max}$	X (10^9 dyn cm^{-2})	T (°K)	$(\rho_X/\rho_0)_{max}$	X (10^9 dyn cm^{-2})	T (°K)	Stress direction
Ga-1(LCR I)	0.40	630±10	2.35	0.68	4.2	3.35	0.54	1.73	[100]
Ga-2(LCR I)	0.04	430±7	2.72	0.86	4.2	3.25	0.57	1.44	[100]
Ga-3(LCR II)	0.40	330±6	1.48	0.87	4.2	2.65	0.71	1.24	[100]
Ga-4(LCR II)	0.04	330±6	2.39	0.75	4.2	9.09	0.68	1.35	[100]
Ga-6(LCR II)	0.40	180±3	2.27	0.83	4.2	5.17	0.60	1.23	[100]
Ga-7(ICR)	0.04	240±4	1.80	0.76	4.2	10.5	1.01	1.25	[100]
Ga-9(ICR)	0.04	220±4	1.71	0.82	4.2	11.2	1.05	1.22	[100]
Ga-11(ICR)	0.04	195±3	3.20	0.86	4.2	23.9	1.29	1.36	[100]
Ga-12(ICR)	0.04	170±3	4.11	1.01	4.2	34.5	1.22	1.23	[100]
Ga-13(ICR)	0.04	165±3	7.18	1.01	4.2	47.2	1.30	1.27	[100]
Ga-14(ICR)	0.04	160±3	6.06	1.13	4.2	31.1	1.27	1.41	[100]
Ga-15(ICR)	0.04	155±3	14.8	1.04	4.2	69.4	1.25	1.31	[100]
Ga-16(ICR)[a]	0.04	155±3	20.8	1.14	4.2	117	1.65	1.30	[100]
Ga-18(ICR)	0.04	142±2	26.5	1.18	4.2	164	1.32	1.28	[100]
Ga-19(ICR)	0.04	138±2	26.1	1.28	4.2	520	1.35	1.22	[100]
Ga-5(LCR II)	0.04	320±6	3.52	1.30	4.2	17.1	1.59	1.58	[111]
Ga-8(ICR)	0.04	320±4	2.75	1.99	4.2	60.8	2.95	1.58	[111]
Ga-10(ICR)	0.04	195±3	5.09	2.28	4.2	180	2.72	1.46	[111]
Ga-17(ICR)	0.04	150±3	38.5	1.93	4.2	1127	2.73	1.27	[111]

[a] Current parallel to [010].

the high-stress region both $\ln\rho_3$ and ϵ_3 are linear functions of $1/X$. However, in this concentration region A_3 is positive. Table IV lists the experimental values of $\epsilon_3(\infty)$, A_3, $\ln\rho_3(\infty)$ and B_3. Ga-6 is included here, rather than at ICR, because it exhibits only ϵ_3 and not ϵ_2, due to its high compensation. The limits of this concentration region are compensation-dependent.

3. *Intermediate-Concentration Region*

In Fig. 5 the resistivity ρ is plotted against $1/T$ for various stresses for Ga-14. In the impurity conduction region the curve exhibits both activation energies ϵ_2 and ϵ_3. Here again, as in the low-concentration regions,

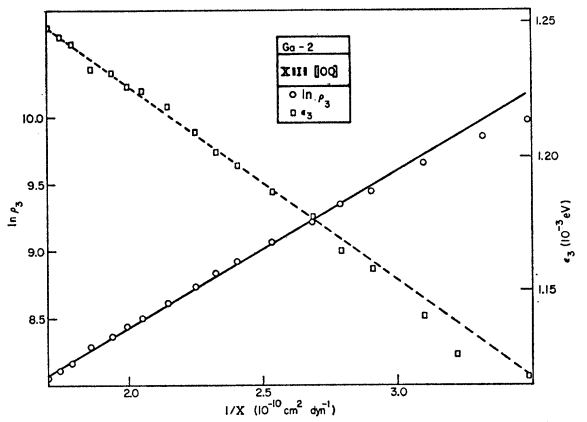

FIG. 4. The values of $\ln\rho_3$ and ϵ_3 of Ga-2 as a function of $1/X$. Both curves are linear in $1/X$ for $X>4\times10^9$ dyn cm^{-2}.

ρ_X/ρ_0 first increases, reaches a maximum and then decreases as the stress is increased. In the ϵ_1 region ρ_X/ρ_0 again decreases montonically. In contrast to the low-concentration regions, however, the temperature dependence of $(\rho_X/\rho_0)_{max}$ is stronger, increasing as R decreases. The stress at which $(\rho_X/\rho_0)_{max}$ occurs becomes slightly larger as the temperature decreases. This is shown in Table III.

It should be noted that both ϵ_2 and ϵ_3 increase at low stresses and then decrease in the high-stress region. Both ϵ_2 and ϵ_3 are linear functions of $1/X$ in the high-stress region and hence one may write

$$\epsilon_i(X)=\epsilon_i(\infty)+A_i/X \quad \text{for} \quad i=2,3. \tag{5}$$

In this concentration range both A_2 and A_3 are positive. It is found that $\ln\rho_2$ decreases only slightly with stress. Although $\ln\rho_3$ decreases with stress it is not linear in $1/X$ for any of the samples measured. Its stress dependence decreases as R decreases.

Table V lists the experimental values of $\epsilon_2(\infty)$, A_2, $\epsilon_3(\infty)$, and A_3. It should be noted that (1) A_2 is equal in sign and, within experimental error,[26] equal in magnitude to A_1 (see Table II), (2) A_2 is concentration independent and (3) A_3 is concentration-dependent, increasing as R decreases. The exceptions to the above statement are samples Ga-18 and Ga-19. N_A for these

[26] The values listed in Table II are somewhat different for Ge doped with Al or with In. Our measurements on Ga acceptors should be compared with those on Al acceptors since the zero-stress ionization energy of Ga acceptors (0.0108 eV) is closer to that of Al (0.0105 eV) than that of In (0.0115 eV).

TABLE IV. Comparison of experimental and theoretical values of $\ln\rho_3(\infty)$, B_3, $\epsilon_3(\infty)$, and A_3.

Sample	K	R (Å)	Experiment $\ln\rho_3(\infty)$	Experiment B_3 (10^{10} dyn cm^{-2})	Theory $\ln\rho_3(\infty)$	Theory B_3 (10^{10} dyn cm^{-2})	Experiment $\epsilon_3(\infty)$ (10^{-3} eV)	Experiment A_3 (10^6 eV dyn cm^{-2})	Theory $\epsilon_3(\infty)$ (10^{-3} eV)	Theory A_3 (10^6 eV dyn cm^{-2})	Stress direction
					Low-concentration region I						
Ga-1	0.40	630±10	+11.65 ±0.30	+1.42 ±0.03	+10.50 ±0.40	+2.10 ±0.40	+0.41 ±0.01	−0.10	+0.42 ±0.02	−0.045 ±0.010	[100]
Ga-2	0.04	430±7	+5.99 ±0.20	+1.22 ±0.03	+5.62 ±0.20	+1.18 ±0.20	+1.37 ±0.03	−0.72 ±0.07	+1.21 ±0.02	−0.27 ±0.05	[100]
					Low-concentration region II						
Ga-3	0.40	330±6	+3.92 ±0.20	+0.99 ±0.02	+3.79 ±0.15	+0.80 ±0.15	+0.44 ±0.02	+0.47 ±0.04	+0.86 ±0.02	−0.31 ±0.06	[100]
Ga-4	0.40	330±6	+2.73 ±0.22	+0.52 ±0.04	+3.79 ±0.15	+0.80 ±0.15	+1.54 ±0.15	+0.47 ±0.05	+1.61 ±0.03	−0.59 ±0.11	[100]
Ga-5	0.04	320±6	+4.08 ±0.15	+0.36 ±0.02	+3.85 ±0.15	+0.47 ±0.15	+1.77 ±0.03	< +0.08	+1.68 ±0.03	−0.29 ±0.10	[111]
Ga-6	0.40	180±3	−1.54 ±0.05	+0.89 ±0.03	+0.86 +0.10	+0.32 ±0.06	+0.04 ±0.01	+1.06 ±0.03	+1.90 ±0.03	−1.91 ±0.35	[100]

samples is such that they are already outside the intermediate concentration range. This can be seen in Fig. 1. At $R\approx 140$ Å the curve has a small tail where the behavior of the activation energies is different from that at larger R. This tail has also been observed for P and As impurities.[2]

For Ga-16 the current was measured perpendicular to the stress direction to determine whether the stress dependence of ϵ_2 and ϵ_3 is isotropic. The results are listed in Table V and should be compared to those of Ga-15. One observes that $\epsilon_2(\infty)$ and A_2 are isotropic which suggests that the conduction process in the ϵ_2 region is thermally activated. A_3 and $\epsilon_3(\infty)$ appear to be slightly anisotropic but since these factors are more sensitive to concentration than $\epsilon_2(\infty)$ and A_2 the apparent anisotropy could be caused by a small concentration difference between Ga-15 and Ga-16. For samples Ga-7 and Ga-9, in the high-stress region, $\ln\rho$ versus $1/T$ is not linear in the ϵ_3 region and hence the activation energy could not be determined. Figure 6 illustrates this behavior which has also been observed in n-Ge.[2] It is interesting to note that although at zero stress one observes no ϵ_2 region it appears at high stresses.

TABLE V. Experimental values of $\epsilon_2(\infty)$, A_2, $\epsilon_3(\infty)$, and A_3.

Sample	R (Å)	$\epsilon_2(\infty)$ (10^{-3} eV)	A_2 (10^6 eV dyn cm^{-2})	$\epsilon_3(\infty)$ (10^{-3} eV)	A_3 (10^6 eV dyn cm^{-2})	Stress direction
Ga-7	240±4	+0.49 ±0.02	+10.4 ± 0.4	...	...	[100]
Ga-9	220±4	+0.10 ±0.02	+10.8 ± 0.3	...	...	[100]
Ga-11	195±3	−0.62 ±0.02	+10.6 ± 0.3	+0.40 ±0.03	+3.1 ±0.1	
Ga-12	170±3	−0.96 ±0.02	+10.9 ±0.03	−0.11 ±0.03	+4.3 ±0.1	[100]
Ga-13	165±3	−1.16 ±0.02	+10.6 ± 0.3	−0.41 ±0.03	+5.4 ±0.2	[100]
Ga-14	160±3	−1.19 ±0.02	+10.9 ± 0.3	−0.73 ±0.03	+6.6 ±0.2	[100]
Ga-15	155±3	−1.44 ±0.02	+10.8 ± 0.3	−1.01 ±0.03	+7.6 ±0.2	[100]
Ga-16[a]	155±3	−1.43 ±0.02	+10.6 ± 0.3	−1.26 ±0.03	+8.6 ±0.2	[100]
Ga-18	142±2	−1.34 ±0.02	+ 8.7 ± 0.2	−1.19 ±0.03	+7.2 ±0.2	[100]
Ga-19	138±2	−1.17 ±0.02	+ 6.5 ± 0.2	−0.82 ±0.03	+4.7 ±0.2	[100]
Ga-17	150±3	+0.16 ±0.02	+10.8 ± 0.3	...	...	[111]

[a] Current parallel to [010].

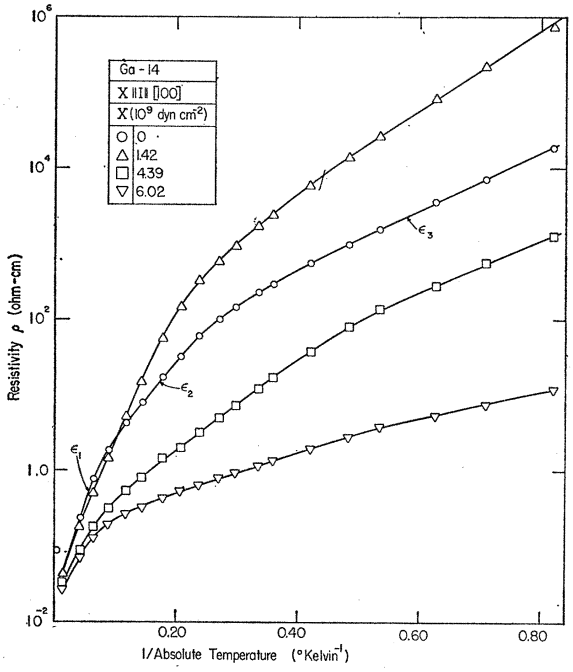

FIG. 5. Resistivity of Ga-14 for various [100] compressional stresses as a function of $1/T$. In the impurity-conduction region, which extends from about 10°K to the lowest temperatures, both ϵ_2 and ϵ_3 are present.

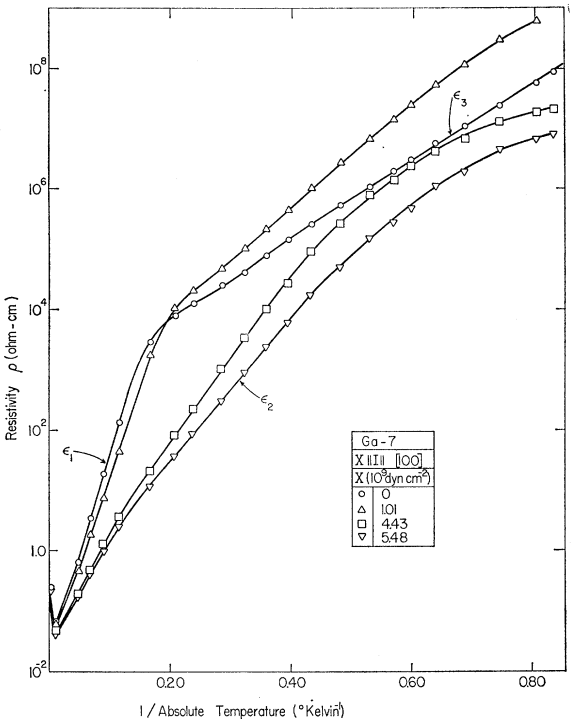

FIG. 6. Resistivity of Ga-7 for various [100] compressional stresses as a function of $1/T$. For large stresses the curve is not linear in the ϵ_3 region and the activation energy ϵ_2, which is absent at zero stress, appears.

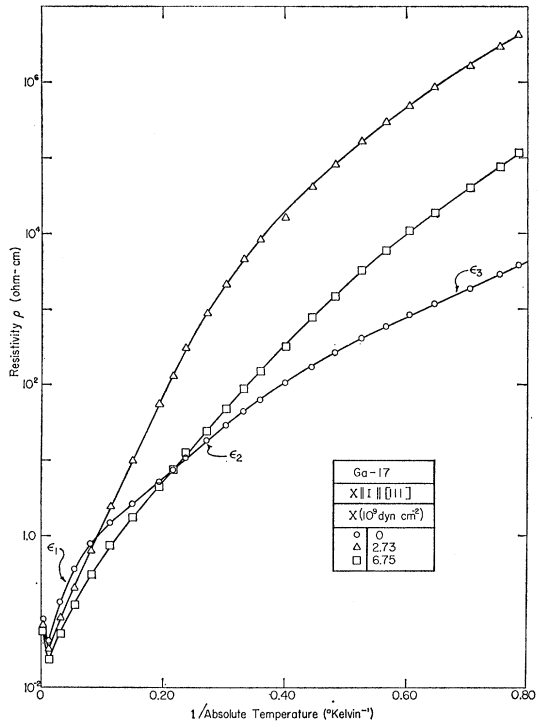

FIG. 7. Resistivity of Ga-17 for various [111] compressional tresses as a function of $1/T$. Except for low stresses the curve is not linear in the ϵ_3 region. Note that in the impurity-conduction region the resistivity for the largest stress applied is greater than the value at zero stress.

B. Stress Parallel to [111]

Figure 7 shows the resistivity ρ as a function of $1/T$ for various stresses for Ga-17. The behavior of the resistivity is similar to that for [100] stress. At low stresses ϵ_2 and ϵ_3 increase and then decrease in the high-stress region. It should be noted that in contrast to [100] stress, for the largest stress applied $\rho_X/\rho_0>1$ in the impurity conduction region. Also, as shown in Table III, the stresses at which $(\rho_X/\rho_0)_{\max}$ occurs are larger than the stresses at which it occurs for [100] stress.

Also for this stress direction A_2 is equal in sign and, within experimental error, magnitude to A_1, as shown in Tables V and II.

At high stresses the $\ln\rho$ versus $1/T$ curve for Ga-17 is not linear in the ϵ_3 region. For Ga-8 and Ga-10 it is not linear in either the ϵ_2 or ϵ_3 region at high stresses.

IV. THEORETICAL DISCUSSION AND COMPARISON WITH EXPERIMENTAL RESULTS

In unstressed p-Ge the effective mass theory of the acceptor wave function is complicated[17–19] because of the degeneracy of the valence bands at $\mathbf{k}=0$. Variational calculations have yielded only approximate solutions[18,19] which have not yet been extended to describe the wave functions at arbitrary stresses. The shear component of a uniaxial stress removes this degeneracy and the bands are separated by an energy proportional to the stress.[15,16,20,21] The hydrostatic pressure component shifts the band edges and acceptor states by the same amount[20] and hence does not affect the wave function. The case for compression along [100] is shown in Fig. 8, where S_{11} and S_{12} are elastic constants and b is the deformation potential for this stress direction. As will be shown below, the separation of the bands by the stress causes the envelope function originating from the upper band to expand with increasing stress in the high-stress region.

At stresses large enough so that the two bands can be considered decoupled the acceptor ground state will be composed solely of Bloch functions from the upper band.[27,28] We shall henceforth refer to this as the "infinite"-stress case. The acceptor ground-state wave function is the product of Bloch functions from the

[27] W. Kohn, in *Solid State Physics*, edited by F. Seitz and D. Turnbull (Academic Press Inc., New York, 1957), Vol. 5, p. 257.

[28] In this discussion we have ignored the $J=\frac{1}{2}$ band split off by the spin-orbit interaction (see Fig. 8). Hasegawa (Ref. 21) has pointed out that the effective-mass tensor of the upper band has an explicit stress dependence due to the interaction of this band with the $J=\frac{1}{2}$ band. This effect has been observed in cyclotron resonance studies of strained Si [J. C. Hensel and G. Feher, Phys. Rev. **129**, 1041 (1963)] and Ge (Ref. 35). In the case of Si the deformation potentials were determined from this effect. It will be shown that the interaction of these two bands is not important in our case.

top of the band and an envelope function $F(r,\infty)$, where ∞ stands for $X=\infty$. Cyclotron resonance studies have shown[29] that for large compressional stress along [100] or [111] the upper band, near $\mathbf{k}=0$, is an oblate ellipsoid whose principal axes coincide with those of the strain tensor. $F(r,\infty)$ satisfies the effective-mass equation

$$\left\{-\left[\frac{\hbar^2}{2m_{\parallel}(\infty)}\right]\frac{\partial^2}{\partial x^2}-\left[\frac{\hbar^2}{2m_{\perp}(\infty)}\right]\left(\frac{\partial^2}{\partial y^2}+\frac{\partial^2}{\partial z^2}\right)-e^2/\kappa r\right\}$$
$$\times F(r,\infty)=\epsilon_1(\infty)F(r,\infty), \quad (6)$$

where $m_{\parallel}(\infty)$ and $m_{\perp}(\infty)$ are the infinite-stress effective masses parallel and perpendicular to the stress direction, respectively, and $\epsilon_1(\infty)$ is the acceptor ionization energy at infinite stress. For [100] stress[16]

$$m_0/m_{\parallel}(\infty)=(A+B) \quad \text{and} \quad m_0/m_{\perp}(\infty)=(A-B/2) \quad (7)$$

and for [111] stresses

$$\text{and} \quad \begin{aligned} m_0/m_{\parallel}(\infty)&=(A+D/\sqrt{3}) \\ m_0/m_{\perp}(\infty)&=(A-\sqrt{3}D/2), \end{aligned} \quad (8)$$

where A, B, and D are the inverse cyclotron mass parameters[30] and m_0 is the free-electron mass.

Equation (6) is not separable and exact solutions have not yet been found. However, at large r, where the potential energy may be neglected compared to the kinetic energy, Eq. (6) can be solved with the result that

$$F(r,\infty)=[\pi a_{\parallel}(\infty)a_{\perp}(\infty)^2]^{-1/2}$$
$$\times\exp\left\{-\left[\frac{x^2}{a_{\parallel}(\infty)^2}+\frac{y^2+z^2}{a_{\perp}(\infty)^2}\right]^{1/2}\right\}, \quad (9)$$

where

$$a_i(\infty)=\hbar[2m_i(\infty)\epsilon_1(\infty)]^{-1/2} \quad \text{with} \quad i=\parallel \text{ or } \perp. \quad (10)$$

An approximate solution to Eq. (6), for all r, has been obtained by a variational calculation[31] using Eq. (9) as a trial function and $a_{\parallel}$ and $a_{\perp}$ as the variational parameters. Table VI lists the values of $a_{\parallel}(\infty)$ and $a_{\perp}(\infty)$ (1) as determined from Eqs. (7), (8), and (10) using the experimental values of A, B, D,[30] and of $\epsilon_1(\infty)$ (see Table II) and (2) as determined from the variational calculation. In the limit of $m_{\perp}/m_{\parallel}=1$ the value of a (∞) determined from Eq. (10) will of course be equal to the value determined from the variational calculation, if there is no chemical shift.[32] Hence, for values of $m_{\perp}/m_{\parallel}$ not too different from unity the two means of determining $a_{\parallel}(\infty)$ and $a_{\perp}(\infty)$ will yield approximately similar results. For [100] stress, since $m_{\perp}/m_{\parallel}=2.45$ and the infinite-stress chemical shift, $\Delta_c(\infty)$,[16] is only 10% of $\epsilon_1(\infty)$, the agreement is good. For [111] stress, since $m_{\perp}/m_{\parallel}=3.18$ and $\Delta_c(\infty)$ is at least 25% of $\epsilon_1(\infty)$ the discrepancy is greater. Hence, for stress along [100] Eq. (10) can be considered a good approximation at large distances from the impurity ion.

TABLE VI. Comparison of $a_{\parallel}(\infty)$ and $a_{\perp}(\infty)$ as determined from Eq. (10) and a variational calculation.

	Eq. (10)	Variational calculation[a]	Stress direction
$a_{\parallel}(\infty)$	132 Å	129 Å	[100]
$a_{\perp}(\infty)$	84 Å	93 Å	[100]
$a_{\parallel}(\infty)$	121 Å	130 Å	[111]
$a_{\perp}(\infty)$	69 Å	86 Å	[111]

[a] Reference 31.

At infinite stress the upper and lower valence bands can be considered decoupled but when the stress is reduced the bands will interact causing a perturbation, which to first order is given[16] by $Z(\mathbf{k})/E_s$. E_s is the energy separation between bands. For [100] compressional stress[16]

$$Z(\mathbf{k})=3B^2(k_y^2+k_z^2)[k_x^2+1/4(k_y^2+k_z^2)]$$
$$+C^2(k_x^2k_y^2+k_y^2k_z^2+k_z^2k_x^2), \quad (11)$$

$$E_s=2b(S_{11}-S_{12})X=2.44\times10^{-12}\,bX, \quad (12)$$

and for [111] compressional stress

$$Z(\mathbf{k})=(2B^2+D^2/3)k_x^2(k_y^2+k_z^2)$$
$$+(B^2/4+D^2/6)(k_y^2+k_z^2)^2, \quad (13)$$

$$E_s=(S_{44}d/\sqrt{3})X=0.838\times10^{-12}\,dX, \quad (14)$$

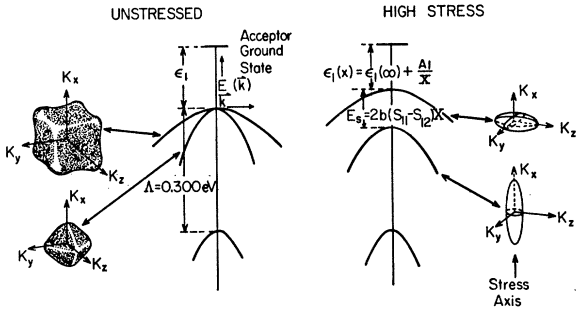

FIG. 8. The left side shows the valence bands of unstressed germanium near $\mathbf{k}=0$. The warped energy surfaces are shown schematically. The acceptor ionization energy is ϵ_1. The right side shows the split valence bands at high stresses for uniaxial compressional stress along [100]. The band splitting at $\mathbf{k}=0$ is denoted by E_s. The energy surfaces near $\mathbf{k}=0$ are an oblate ellipsoid (upper band) and a prolate ellipsoid (lower band) both having axial symmetry about the stress direction. The stress dependence of ϵ_1 is shown.

[29] T. R. Loree, M. H. Halloran, and R. N. Dexter, Bull. Am. Phys. Soc. **6**, 426 (1961).
[30] B. W. Levinger and D. R. Frankl, J. Phys. Chem. Solids **20**, 281 (1961).
[31] R. W. Keyes, IBM J. Res. Develop. **5**, 65 (1961).
[32] The chemical shift Δ_c is the difference between the experimental and calculated values of the ionization energy ϵ_1 and is a measure of the failure of the effective-mass approximation (and the associated variational calculation) to describe the impurity ground state.

where $C=(D^2-3B^2)^{1/2}$, S_{11}, S_{12}, and S_{44} are elastic constants,[33] and b and d are deformation potentials.[16]

$Z(\mathbf{k})/E_s$ may be considered as a correction term to Eq. (6), the infinite stress effective-mass Hamiltonian, and following Kohn and Luttinger[34] we will assume that the effect of this correction term on the envelope function can be included in the variational parameters $a_{\parallel}$ and $a_{\perp}$. That is,

$$a_i(X)=\hbar[2m_i(X)\epsilon_1(X)]^{-1/2} \quad \text{with} \quad i=\parallel \text{ or } \perp. \tag{15}$$

The effect of stress on ϵ_1 is calculated by first-order perturbation theory to be[15]

$$\epsilon_1(X)=\epsilon_1(\infty)+\langle F(\mathbf{r},\infty)|Z(-i\nabla)/E_s|F(\mathbf{r},\infty)\rangle =\epsilon_1(\infty)+A_1/X. \tag{16}$$

A_1 and $\epsilon_1(\infty)$ have been measured for compressional stress along [100] and [111] for Al and In impurities and are listed in Table II. The deformation potentials b and d were determined from these measurements.[16]

The stress dependence of $m_{\parallel}$ and $m_{\perp}$ was calculated by Hasegawa[21] and measured by Dexter.[35] It is found experimentally that in the high-stress region, for both [100] and [111] compression, $m_{\parallel}$ is almost independent of stress while $m_{\perp}$ is increasing with stress. For a change of stress from 4×10^9 dyn cm^{-2} to 7×10^9 dyn cm^{-2}, $m_{\parallel}$ decreases by about 1% while $m_{\perp}$ increases by about 10%.[36] From this two conclusions can be drawn: (i) the stress dependence of $a_{\parallel}$ is caused almost entirely by the stress dependence of ϵ_1 and hence from Eqs. (15) and (16) one obtains

$$a_{\parallel}(X)=a_{\parallel}(\infty)\{1-[A_1/2\epsilon_1(\infty)](1/X)+\cdots\}, \tag{17}$$

where $a_{\parallel}(\infty)$ is given by Eq. (10), and (ii) the stress dependence of $a_{\parallel}$ is greater than that of $a_{\perp}$. Since $a_{\parallel}$ is larger and has a greater stress dependence than $a_{\perp}$ the effects which have been observed are caused primarily by $a_{\parallel}$.

Equation (17) can be verified by investigating the stress dependence of $\ln\rho_3$, at high stresses, in LCR I as will be shown below.

A. High-Stress Region ($X>4\times10^9$ dyn cm^{-2})

1. Low-Concentration Region I

An expression for the resistivity has been calculated by MA[8] based on the assumption that the overlap of wave functions of neighboring impurity sites is small enough so that the resonance energy of a neighboring pair of acceptors is much smaller than their difference in potential energy arising from the spatial variation in local fields produced by nearby ionized acceptors and donors. The holes are then well localized and conduction occurs when an acceptor tunnels from an occupied to an unoccupied site with the emission or absorption of a phonon to conserve energy. Their final expression for the resistivity is, in our notation,

$$\rho=\rho_3\exp(\epsilon_3/kT), \tag{18}$$

where

$$\rho_3=C(R/a_{\parallel})[1+18.2(a_{\parallel}/R)^{3/2}]\times\exp[1.09(R/a_{\parallel})^{3/2}], \tag{19}$$

$$C=4.55\times10^2\,\ell_e(\alpha/8)^{1/2}\kappa^2 n\rho_0 v^5\hbar^4 a_{\parallel}{}^3/e^6E_1{}^2, \quad \alpha=(a_{\parallel}/a_{\perp})^2-1. \tag{20}$$

The effects of the excited states are contained in ℓ_e; these are unimportant in our case and hence $\ell_e=1$. The number of valence band maxima n is equal to one, κ is the static dielectric constant (=16 for Ge), ρ_0 the density and v the velocity of sound in the crystal. E_1 is an average deformation potential which takes into account both shearing strain and dilation.

Pre-exponential factor ρ_3. The stress dependence of ρ_3 is caused primarily by the stress dependence of $a_{\parallel}$. The predominant effect will come from the exponential term of Eq. (19) and hence one may write

$$\ln\rho_3(X)=1.09[R/a_{\parallel}(X)]^{3/2}+\ln D_3(X), \tag{21}$$

where

$$D_3(X)=C(X)[R/a_{\parallel}(X)]\{1+18.2[a_{\parallel}(X)/R]^{3/2}\}.$$

Any changes in the second term of Eq. (21) will be very small compared to the first term and hence $\ln D_3$ is evaluated at infinite stress. Combining Eqs. (17) and (21), one obtains

$$\ln\rho_3(X)=\ln\rho_3(\infty)+B_3/X, \tag{22}$$

where

$$\ln\rho_3(\infty)=1.09[R/a_{\parallel}(\infty)]^{3/2}+\ln D_3(\infty) \tag{23}$$

and

$$B_3=1.09[R/a_{\parallel}(\infty)]^{3/2}[3A_1/4\epsilon_1(\infty)]. \tag{24}$$

Therefore, in the high-stress region $\ln\rho_3$ is a linear function of $1/X$ with a positive sign for B_3. Listed in Table IV are the theoretical values of $\ln\rho_3(\infty)$ and B_3 calculated from Eqs. (23) and (24) using the values of the parameters listed in Table VII.

As seen in Table IV the theory gives the correct sign for B_3 and accounts well for the magnitude of $\ln\rho_3(\infty)$ and B_3. This agreement indicates that in this region the stress dependence of the Bohr radius is given by Eq. (17).

Activation energy ϵ_3. The activation energy ϵ_3 was first explained by Mott[11] as due to the Coulomb interaction of the carriers with the compensating impurity ion. The theory of MA[8] gives

$$\epsilon_3=(e^2/\kappa R)f(K), \tag{25}$$

---

[33] M. E. Fine, J. Appl. Phys. **26**, 862 (1955).
[34] W. Kohn and J. M. Luttinger, Phys. Rev. **97**, 883 (1955).
[35] R. N. Dexter (private communication).
[36] In the stress region discussed the stress dependence of the effective masses is caused by the interaction of the upper band with the band split off by the spin-orbit interaction (Ref. 21). As will be shown, $m_{\parallel}$ is a more important parameter than $m_{\perp}$ so that the observed weak stress dependence of $m_{\parallel}$ in this stress region indicates that we can neglect the interaction of these two bands.

TABLE VII. Values of parameters used to calculate $\ln\rho_3(\infty)$, B_3, $\epsilon_3(\infty)$, and A_3.

	[100] Stress	[111] Stress
$a_{\parallel}(\infty)$	132 Å	121 Å
$a_{\perp}(\infty)$	84 Å	69 Å
A_1	$(11.7\pm1.6)\times10^6$ eV dyn cm^{-2} [a]	$(8.4\pm2.1)\times10^6$ eV dyn cm^{-2} [a]
$\epsilon_1(\infty)$	$(4.75\pm0.15)\times10^{-3}$ eV[a]	$(6.30\pm0.15)\times10^{-3}$ eV[a]
v	4.92×10^5 cm sec^{-1} [b]	4.92×10^5 cm sec^{-1} [b]
ρ_0	5.32 g cm^{-3}	5.32 g cm^{-3}
E_1	4 eV	4 eV

[a] Reference 16.
[b] H. J. McSkimin, J. Appl. Phys. 24, 988 (1953).

where R is the average separation between majority impurities, κ is the static dielectric constant, and $f(K)$ is a function of the compensation ratio K. For $0<K<0.20$ it has been found by MA that $f(K)=(1-1.35K^{1/3})$. Equation (25) is based on the assumption that the charge distribution of an acceptor is spherically symmetric about its ion core and hence the interaction with the compensating impurity ion is just the classical Coulomb potential and independent of wave function size. However, if the charge distribution is cigar shaped, as it is at high stresses, the interaction between the hole and donor ion is given by

$$\int\psi^*(\mathbf{r})[-e^2/\kappa r_{\mathrm{HD}}]\psi(\mathbf{r})d\tau\,, \tag{26}$$

where $\psi(\mathbf{r})$ is the wave function of the hole given by Eq. (9) and r_{HD} is the distance between the hole and donor ion.

This integral has not yet been evaluated exactly but certain approximations can be made which bring out the essential features. If the line connecting the acceptor and donor ions lies along the stress direction, a multipole expansion of Eq. (26) gives

$$-(e^2/\kappa R)\{1+[(a_{\parallel}{}^2-a_{\perp}{}^2)/R^2]+\cdots\}\,. \tag{27}$$

Hence, because of the anisotropy of the charge distribution some correction terms are added to the Coulomb term $e^2/\kappa R$ which now makes the interaction dependent on the size and shape of the acceptor wave function. The stress dependence of ϵ_3 can be approximated by assuming that it is caused only by the stress dependence of $a_{\parallel}$ and by retaining only the first term of Eq. (27). One then obtains from Eqs. (17), (25), and (27)

$$\epsilon_3(X)\approx\epsilon_3(\infty)+A_3/X\,, \tag{28}$$

where

$$\epsilon_3(\infty)=(e^2/\kappa R)f(K)\{1+[a_{\parallel}(\infty)^2-a_{\perp}(\infty)^2]/R\} \tag{29}$$

and

$$A_3=-(e^2/\kappa R)f(K)[a_{\parallel}(\infty)^2A_1/R^2\epsilon_1(\infty)]\,. \tag{30}$$

Since the sign of A_3 is negative ϵ_3 should increase with increasing stress. A_3 and $\epsilon_3(\infty)$ should be dependent on concentration and compensation.

Table IV lists the values of $\epsilon_3(\infty)$ and A_3 calculated from Eqs. (29) and (30) using the values of the parameters listed in Table VII and[8] $f(K)=0.289$ for $K=0.40$. The theory accounts qualitatively for $\epsilon_3(\infty)$ and A_3. Considering that only the first term of Eq. (27) was retained it is not surprising that the theoretical values are low. However, the essential features, i.e., the negative sign of A_3 and the concentration and compensation dependence of $\epsilon_3(\infty)$ and A_3, are brought out.

2. *Low-Concentration Region II*

In Table IV are listed the theoretical values of $\ln\rho_3(\infty)$, B_3, $\epsilon_3(\infty)$, and A_3 as calculated from Eqs. (23), (24), (29), and (30) using the values listed in Table VII. For ρ_3 the agreement is fairly good except for Ga-6, for which the agreement is only qualitative. This indicates that MA theory for ρ_3 is still valid in this concentration region. However, the theory gives the wrong sign for A_3 and an incorrect concentration dependence for $\epsilon_3(\infty)$. The fact that the theory is unable to account for the stress dependence of ϵ_3 is not surprising because, as shown in Fig. 1, the theory no longer accounts for the concentration dependence of ϵ_3 in this region. Since the overlap of acceptor wave functions in LCR II is greater than in LCR I, ϵ_3 may no longer be determined only by the Coulomb interaction of the acceptors with the ionized minority impurities so that it may be necessary to take into consideration the resonance energy between neighboring sites, which was neglected in LCR I. As far as the activation energy is concerned these samples should be included in ICR because of the positive sign of A_3 and the concentration dependence of $\epsilon_3(\infty)$.

3. *Intermediate-Concentration Region*

In this concentration region impurity conduction exhibits both ϵ_2 and ϵ_3. Little is known about either of these processes. As shown in Fig. 1, the R dependence of ϵ_3 no longer agrees with the prediction of MA. The reason for the breakdown of the theory for concentrations greater than those in LCR I has already been discussed. The stress dependence of ϵ_3 in this region, its increase at low stresses and decrease in the high-stress region, suggests that it is a function of the effective Bohr radius. However, we have found that it is not possible to express ϵ_3 as a function of only R/a. Since there is no theory for ϵ_3 in this concentration region no comparison with the experimental results could be made.

It has been found that ϵ_2 is a sensitive function of R (see Fig. 1) and the effective Bohr radius.[2] Several theories have been proposed to explain this conduction process[12–14] and in the following sections these theories will be outlined and compared with the experimental results for both the high- and low-stress regions.

Mikoshiba's theory of ϵ_2. On the left side of Fig. 9 are shown some randomly distributed neutral acceptors A. At low temperatures most of the holes are in the

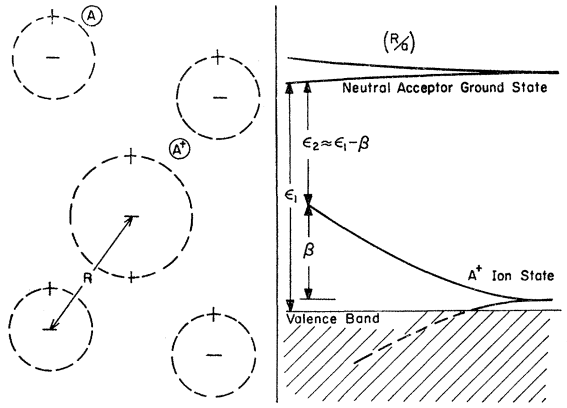

FIG. 9. The left side shows schematically some randomly distributed acceptors, A, and a positively ionized acceptor, A^+. The right side shows schematically the valence band of germanium and the bands formed by the positively ionized A^+ states and neutral acceptor ground state as a function of the overlap parameter R/a.

acceptor ground state. However, due to thermal excitations it is possible to form a positively charged hydrogen-like ion A^+. Because the hole wave functions of the A^+ ion states are spread out further than the hole wave function of the neutral acceptor ground state, the exchange interaction between A^+ states is stronger, causing an A^+ band[37] to be formed in which the holes will be considerably more mobile than in the narrow band formed by the neutral acceptor ground state.

The energy of the isolated A^+ state is very nearly equal to the neutral acceptor ionization energy ϵ_1, as shown on the right side of Fig. 9. Because of the exchange interaction β, the energy of the A^+ state is lowered. The activation energy ϵ_2 is then assumed to be the energy gap between the neutral acceptor ground state and the bottom of the A^+ band. Neglecting the slight broadening of the neutral acceptor ground state and the small energy difference between ϵ_1 and the energy of the isolated A^+ state, one obtains

$$\epsilon_2 \approx \epsilon_1 - \beta. \tag{31}$$

In order to calculate β, Mikoshiba approximates the wave function of the A^+ state by a screened $1s$ hydrogen wave function and the interaction potential $U(\mathbf{r})$ by a screened Coulomb interaction. That is,

$$\beta = n\int \psi_{A^+}(\mathbf{r}_i) U(\mathbf{r}_i) \psi_{A^+}(\mathbf{r}_j) d\tau,$$

$$= (ne^2 s^2/\kappa a)(1+sR/a)\exp[-(sR/a)], \tag{32}$$

where

$$\psi_{A^+}(\mathbf{r}) = (s^3/\pi a^3)^{1/2} \exp[-(sr/a)],$$

$$U(\mathbf{r}) = se^2/\kappa r.$$

[37] The term band has been used rather loosely because the impurity atoms are assumed to be randomly distributed rather than in a periodic sublattice. However, the term band can still be used in the sense of a distribution of energy levels.

It should be noted that the wave functions are assumed to be spherically symmetric in contrast to the cigar-shaped wave functions which were used in the discussion of low-concentration impurity conduction. This assumption will be justified in Sec. IV-A-4.

By Slater rules[38] the screening parameter s equals 0.70 for the isolated A^+ ion. The parameter n is the number of nearest neighbors and may be considered as adjustable.

In Fig. 10 the experimental values of $\epsilon_2(\infty)$, for [100] stress, are plotted as a function of R. The solid line has been calculated from Eqs. (31) and (32) using the values shown in that figure. The values of n and $a(\infty)$ were obtained in the following manner. The extrapolation of the experimental curve of $\epsilon_2(\infty)$ versus R to $R=0$ is found to be -5×10^{-3} eV, which happens to be $-\epsilon_1(\infty)$. Therefore, from Eq. (31), β should equal $2\epsilon_1(\infty)$ at $R=0$. Since $s=0.70$, if we assume $n=2$ and $\epsilon_1(\infty)$ to be given by

$$\epsilon_1(\infty) = e^2/2\kappa a(\infty) \tag{33}$$

then at $R=0$, from Eq. (32), $\beta = 0.98\, e^2/\kappa a(\infty) \approx 2\epsilon_1(\infty)$. The value of $a(\infty)$ was then determined from Eq. (33) using $\epsilon_1(\infty) = 4.9\times10^{-3}$ eV.

From Eq. (31) one obtains

$$\partial\epsilon_2/\partial(1/X) \approx \partial\epsilon_1/\partial(1/X) - \partial\beta/\partial(1/X) \tag{34}$$

and hence from Eqs. (5) and (16) it is found that

$$A_2 \approx A_1 - \partial\beta/\partial(1/X)\,|_{X=\infty}. \tag{35}$$

As shown in Tables V and II, it has been found that A_2 (1) is concentration-independent and (2) is equal in sign and, within experimental error, equal in magnitude to A_1. In Table VIII are listed the values of

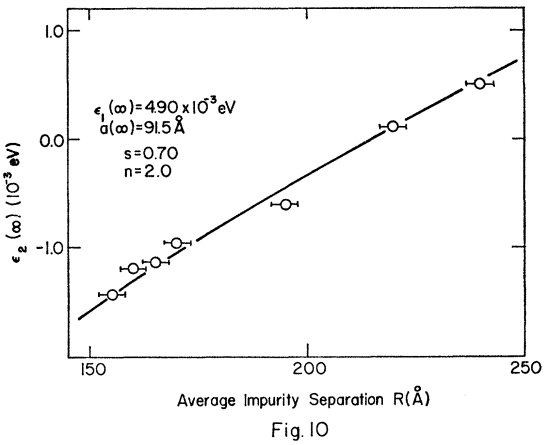

FIG. 10. The experimental values of $\epsilon_2(\infty)$, for [100] compressional stresses, plotted as a function of average impurity separation R. The solid line has been calculated from Eqs. (31) and (32) using the values shown in the figure. Note that $\epsilon_2(\infty)$ is an almost linear function of R.

[38] See for example, C. A. Coulson, *Valence* (Oxford University Press, London, 1952), p. 40.

TABLE VIII. Theoretical values of $\partial\beta/\partial(1/X)|_{X=\infty}$ and A_2 for different values of R.

R (Å)	$\partial\beta/\partial(1/X)\|_{X=\infty}$ (10^6 eV dyn cm^{-2})	A_2 (10^6 eV dyn cm^{-2})
240	−1.80	13.5
220	−0.59	12.3
195	+1.27	10.4
170	+3.52	8.2
165	+4.02	7.7
160	+4.54	7.2
155	+5.03	6.7

$\partial\beta/\partial(1/X)|_{X=\infty}$ and A_2, for different values of R, calculated from Eqs. (32), (43), and (35) using the values of n, $\epsilon_1(\infty)$, and $a(\infty)$ shown in Fig. 10 and $A_1=11.7\times10^6$ eV dyn cm^{-2}. Although there is a qualitative agreement for A_2 the theory predicts a concentration dependence which is considerably greater than the experimental error. The conduction process is assumed to be thermally activated which explains the observed isotropy of ϵ_2. The theory accounts quite well for the dependence of $\epsilon_2(\infty)$ on R under the assumptions mentioned.

Mikoshiba's theory also accounts qualitatively for the increase of ϵ_2 at low stresses, as shown in Figs. 5 and 7, if it is assumed that in the low-stress region the effective Bohr radius is decreasing with increasing stress. Since the changes in ϵ_1 are small at low stresses[16] (for $X=1\times10^9$ dyn cm^{-2} ϵ_1 has decreased about 10% from its zero-stress value), Eqs. (31) and (32) account for the increase of ϵ_2.

It should be pointed out that the concentration independence of A_2 and the observed agreement between A_2 and A_1 means that in the high-stress region the stress dependence of ϵ_2 is due only to the change in ϵ_1 and not a change in the effective Bohr radius. The dependence of ϵ_2 on the effective Bohr radius is illustrated by its behavior at low stresses.

Frood's theory of ϵ_2. Frood[13] suggests that the conduction takes place in the lower tail of the valence band which includes the delocalized excited impurity states. He finds that the effective ionization ϵ_2 decreases with decreasing impurity separation and increasing temperature. This model shows a distinct stress dependence through the shift in the ground state and might thus explain the observed agreement between A_2 and A_1. The proposed mechanism is thermally activated thus explaining the observed isotropy of ϵ_2. The theory is not sufficiently developed to quantitatively compare it to the observed dependence of $\epsilon_2(\infty)$ on R. As in Mikoshiba's theory, ϵ_2 is the difference between ϵ_1 and an exchange energy (although in this theory the exchange energy is due to the interaction of the excited states of the neutral acceptor). This might explain the low-stress behavior of ϵ_2 but encounters difficulty in accounting for the concentration independence of A_2. In addition to this discrepancy Frood's theory has not been able to account for certain results of other experiments on impurity conduction.[2]

Mycielski's theory of ϵ_2. Mycielski[14] proposes that the conduction may be due to a hopping over, as opposed to a tunneling through, the Coulomb barrier separating an occupied majority ion from an empty one. Figure 1 of Ref. 14 illustrates how the activation energy ϵ_2 is obtained in this proposed mechanism. The energy of the carrier in the ground state of the impurity center, taking into account the interaction with the ionized center, is

$$\epsilon_1=-\epsilon_1{}^0-e^2/\kappa R, \tag{36}$$

where $\epsilon_1{}^0$ is the ionization energy of the isolated impurity and R is the separation between impurity centers. The energy at the top of the potential barrier, which is midway between the two centers, is $E_2=-4e^2/\kappa R$. The activation energy $\epsilon_2=E_2-E_1$ and therefore

$$\epsilon_2=\epsilon_1{}^0-3e^2/\kappa R. \tag{37}$$

Mycielski further assumes that the majority centers form an impurity sublattice in the crystal and hence

$$1/R=SN^{1/3}, \tag{38}$$

where S is a parameter depending on the type of sublattice, but never far from unity, and N is the concentration of majority impurities. From Eqs. (37) and (38) one obtains

$$\epsilon_2=\epsilon_1{}^0-(3e^2/\kappa)SN^{1/3}. \tag{39}$$

Figure 2 of Ref. 14 shows ϵ_2, for zero stress, plotted against $N^{1/3}$. For $N^{1/3}=0$ it is found that $\epsilon_2=\epsilon_1{}^0$, in accordance with Eq. (37). From this curve a value of $S=0.88$ is obtained.

Equation (39) predicts a linear relationship between ϵ_2 and the acceptor ionization energy and hence would explain the observed agreement between A_2 and A_1. The second term of Eq. (39) is stress-independent which would account for the concentration independence of A_2. (One could argue that the Coulomb interaction is stress-dependent, as was the case at low concentrations. However, as will be shown in Sec. IV-A-4 the charge distribution of the carrier at intermediate concentrations is spherically symmetric and hence the Coulomb interaction is stress-independent.)

When the experimental values of $\epsilon_2(\infty)$ are plotted against $N^{1/3}$ it is found that $\epsilon_2(\infty)=4.1\pm0.4\times10^{-3}$ eV, which is approximately $\epsilon_1(\infty)$, at $N^{1/3}=0$. However, S as determined from the slope of the curve is 0.52 ±0.05. While it is true that the stress distorts the lattice slightly it is difficult to explain such a large change in S on the basis of this model. Also, since the second term of Eq. (39) is stress-independent the theory does not account for the increase of ϵ_2 at low stresses. Another discrepancy with this model is the prediction that the ionization energy increases with decreasing R [see Eq. (36)]. Experimentally, it is found[4] to decrease slightly with decreasing R.

4. Transition to Metallic Conduction

The critical impurity separation R_c at which the transition from nonmetallic to metallic conduction occurs is defined by $\epsilon_2=0$. Since $\epsilon_2(\infty)$ is an almost linear function of R, as shown in Fig. 10, and since A_2 is concentration-independent, one can write in the high-stress region

$$\epsilon_2(R,X)=-\alpha+\gamma R+A_2/X. \quad (40)$$

This yields

$$R_c(X)=R_c(\infty)\{1-[A_2/\gamma R_c(\infty)](1/X)\}, \quad (41)$$

where

$$R_c(\infty)=\alpha/\gamma.$$

According to Mott and Twose[5] R/a at which metallic conduction occurs is a constant. Therefore, one obtains

$$\frac{R_c(X)}{R_c(\infty)}=\frac{a(X)}{a(\infty)}=1-\left(\frac{A_2}{\alpha}\right)\left(\frac{1}{X}\right). \quad (42)$$

Because of the equality of A_2 and A_1 and since $\alpha\approx\epsilon_1(\infty)$ one obtains from Eqs. (42) and (16)

$$a(X)/a(\infty)=\epsilon_1(\infty)/\epsilon_1(X). \quad (43)$$

This relation between the effective Bohr radius and the ionization energy indicates that the potential energy term in the effective-mass Hamiltonian [Eq. (6)] dominates the kinetic-energy term in this case. The use of the term "effective Bohr radius" for the a's of Eqs. (43) and (9) is extensive in discussions of impurities in semiconductors. Strictly speaking the term Bohr radius has meaning only for the hydrogen problem. In the case of impurities in semiconductors the effective-mass Hamiltonian differs from the hydrogen Hamiltonian because of the anisotropy of the masses (other correction terms such as the central cell potential and interaction of other bands may also be present). In this case the correct wave function will not be equal to the wave function of the hydrogen problem. It has been shown that the correct wave function may be approximated by Eq. (9) for distances far from the impurity center. However, in contrast to the hydrogen problem, the values of $a_{\parallel}$ and $a_{\perp}$ and the ratio $a_{\parallel}/a_{\perp}$ will vary with r. For distances far from the impurity center $a_{\parallel}/a_{\perp}\rightarrow(m_{\perp}/m_{\parallel})^{1/2}$ while at small r, where the isotropic potential energy term becomes large, $a_{\parallel}/a_{\perp}\rightarrow 1$. In discussions of impurity conduction, which depends on the overlap of wave functions of neighboring impurities, the a's which appear in the overlap expressions are those corresponding to the distance from the impurity center where the integrand of the overlap integral has its maximum. In this sense it is possible to label a as "an effective Bohr radius" and talk about its properties far from the impurity center (low concentrations) or at small distances (high concentrations). Therefore, at these high concentrations the relation of Eq. (43) is expected because the maximum contribution to the overlap integral comes from parts of the wave function which are close to the impurity center. In this region the wave function is nearly isotropic which justifies the assumption on which Mikoshiba's theory is based.

Further evidence for the fact that at these high concentrations Eq. (43) is a better approximation than Eq. (17) is also found in n-Ge doped with As, P, or Sb.[3] There the ratio of the effective Bohr radii of the different donors as determined experimentally agree much better with those calculated from Eq. (43) than with those quoted, which were determined from Eq. (17).

Figure 10 shows that $\epsilon_2(\infty)=0$ at $R=215$ Å. Using this value for $R_c(\infty)$ and $a(\infty)=91.5$ Å we find that $R/a=2.35$, which agrees favorably with the values of R/a found for n-Ge.[3]

B. Low-Stress Region ($X<3\times10^9$ dyn cm^{-2})

For low concentrations the primary effect of the stress is to change ρ_3 rather than ϵ_3 and hence $(\rho_X/\rho_0)_{\max}$ has only a weak temperature dependence, as can be seen in Table III.

In the intermediate-concentration region the predominant effect of the stress is an increase of the activation energies ϵ_2 and ϵ_3, as shown in Figs. 5 and 7. Therefore, the temperature dependence of $(\rho_x/\rho_0)_{\max}$ in this concentration region is greater than at low concentrations, as shown in Table III. Because of the rapid decrease of ϵ_2 and ϵ_3 with decreasing R, the relative change of the activation energies with stress becomes greater as R decreases and hence $(\rho_X/\rho_0)_{\max}$ becomes more temperature-dependent as R decreases.

Since it has been shown that an expanding effective Bohr radius causes ρ_3 and ϵ_2 to decrease, the increase in these quantities at low stresses indicate that the effective Bohr radius in this stress region is contracting with increasing stress.

V. CONCLUSIONS

Since uniaxial stress changes the size and shape of the impurity wave function it has proven to be a powerful tool in the investigation of impurity conduction, particularly at high stresses where the wave function is relatively simple.

In LCR I the extension of the theory of MA to include nonspherical charge distributions together with the acceptor wave function calculated from the effective-mass approximation was able to account for the observed stress dependence of ρ_3 and ϵ_3.

The results for LCR II indicate that the theory of MA is valid for ρ_3 but not for ϵ_3 in this region.

In ICR the high-stress results have established the linear relation between ϵ_2 and ϵ_1. Although the experimental results were not able to distinguish between Mikoshiba's and Frood's theories of the ϵ_2 process, they are clearly in disagreement with the predictions of Mycielski's theory. A study of the compensation

dependence of ϵ_2 may determine whether the process is due to a band formed by positively charged impurity ions or the excited states of the neutral impurity. It may also be of interest to determine if ϵ_2 and ϵ_1 have a linear relation also for other acceptors in Ge and for p-Si. The experimental results indicate that ϵ_3, in this concentration region, is a function of the effective Bohr radius although the detailed process leading to ϵ_3 has not been established.

The investigation of the transition to metallic conduction yields the stress dependence of the effective Bohr radius. The form of the stress dependence indicates the importance, at high concentrations, of the potential energy term which can be neglected at low concentrations.

The low-stress behavior of the resistivity indicates that the effective Bohr radius is initially decreasing with increasing stress, due to the change in the relative contributions of the two valence bands to the impurity wave function.

ACKNOWLEDGMENTS

The author wishes to thank his sponsor, Dr. H. Fritzsche, for his many helpful suggestions and encouragement through all phases of this work. The general support of the Low Temperature Laboratory of the Institute for the Study of Metals by the National Science Foundation and the U. S. Atomic Energy Commission is gratefully acknowledged.

PHYSICAL REVIEW VOLUME 138, NUMBER 2A 19 APRIL 1965

Paramagnetic Resonance of $^8S_{7/2}$ Ions in CdSe and CdTe

R. S. TITLE
IBM Watson Research Center, Yorktown Heights, New York
(Received 9 June 1964; revised manuscript received 14 December 1964)

Paramagnetic-resonance measurements for Gd^{3+} in CdSe and CdTe are reported. The resonance parameters for Gd^{3+} are compared with those of the isoelectronic ion Eu^{2+} in the same crystals. The b_n^m parameters characterizing the splitting of the $^8S_{7/2}$ ground state are much larger for Gd^{3+} than for Eu^{2+} in both CdSe and CdTe. The g values for Gd^{3+} are significantly lower than those for Eu^{2+}. The presently available theories of the splitting of the $^8S_{7/2}$ state are considered in the interpretation of these results.

INTRODUCTION

IN this paper paramagnetic resonance measurements for Gd^{3+} in the II-VI compounds CdSe and CdTe are reported. Measurements for the isoelectronic ion Eu^{2+} in these crystals have previously been reported.[1]

The literature has very few references to measurements on rare-earth ions in semiconducting crystals. One is led to speculate whether this is due to a lack of previous interest or due, perhaps, to difficulties in incorporating rare-earth ions in these materials. No difficulty was encountered in incorporating Eu or Gd into CdSe and CdTe. However, only negligibly small amounts of Eu or Gd were obtained in ZnSe and ZnTe. This is probably due to the smaller size of the Zn ion as compared to the rare-earth ions.[2,3] The Cd ion, on the other hand, is comparable in size to those of the rare-earth ions.[3] The resonance measurements for Eu and Gd in CdSe and CdTe, as will be shown, provide some information concerning the surroundings of the rare-earth ion. The information is not without ambiguity because of the presently inadequate understanding of the splitting of the $^8S_{7/2}$ state.

Information concerning the surroundings of the rare-earth impurity is obtained from the effect of the crystalline field of the surrounding ions on the electronic ground state of the rare-earth ion. The crystalline field removes some of the degeneracy of the ground state and leads to splittings which for most rare earths are in the optical range (100 to 1000 cm^{-1}). Paramagnetic resonance measurements carried out in the microwave region are therefore limited to the lowest lying level. The measurement of the g tensor of this level is sufficient to determine the symmetry of the rare-earth site, but provides insufficient data to determine the magnitudes of the radial parameters characterizing the crystalline field. In certain cases where the spin lattice relaxation is via an Orbach process,[4] the position of the next highest level may be determined by a measurement of variation of the spin-lattice relaxation time with temperature.

One advantage of working with Eu^{2+} or Gd^{3+} is that they have splittings of their ground states which are in the microwave rather than the optical range. All the data concerning the splittings may therefore be obtained by paramagnetic resonance techniques. There is however, at present, some difficulty in interpreting the splitting of the ground state. The $4f^7$ configuration

[1] R. S. Title, Phys. Rev. **133**, A198 (1964).
[2] R. S. Title, Phys. Rev. **131**, 2503 (1963).
[3] V. M. Goldschmitt, Trans. Faraday Soc. **25**, 253 (1929).
[4] R. Orbach, Proc. Roy. Soc. (London) **A264**, 458 (1961).